ADVANCED ELECTRONIC MATERIALS
www.advelectronicmat.de

Energy-Efficient Hybrid Perovskite Memristors and Synaptic Devices

*Zhengguo Xiao and Jinsong Huang**

New parallel computing architectures based on neuromorphic computing are needed due to their advantages over conventional computation with regards to real-time processing of unstructured sensory data such as image, video, or voice. However, developing artificial neuromorphic system remains a challenge due to the lack of electronic synaptic devices, which can mimic all the functions of biological synapses with low energy consumption. Here it is reported that two-terminal organometal trihalide perovskite (OTP) synaptic devices can mimic the neuromorphic learning and remembering process. Various functions known in biological synapses are demonstrated in OTP synaptic devices including four forms of spike-timing-dependent plasticity (STDP), spike-rate-dependent plasticity (SRDP), short-term plasticity (STP) and long-term potentiation (LTP)), and learning-experience behavior. The excellent photovoltaic property of the OTP devices also enables photo-read synaptic functions. The perovskite synapse has the potential of low energy consumption of femto-Joule/(100 nm)^2 per event, which is close to the energy consumption of biological synapses. The demonstration of energy-efficient OTP synaptic devices opens a new plausible application of OTP materials into neuromorphic devices, which offer the high connectivity and high density required for biomimic computing.

1. Introduction

Neuromorphic computing, combining information processing and remembering, could eliminate the bottleneck of Von-Neumann computing architecture limited by the data transfer speed between memory and central processing unit.[1,2] Nanoscale electronic synaptic device is an emerging research field aiming at emulating biological synapses and is regarded as the basic building blocks for artificial neuromorphic computing systems. Two-terminal memristors or three-terminal transistors can emulate the functions of biological synapses due to their similar transmission characteristics and have been proposed to realize neuromorphic computers.[2–8] The reproducible gradual tuning of resistance/conductivity of the memristor represents the synaptic plasticity, which is the basis of remembering and learning in the brain.[1] However, not all the functions discovered in biological synapses have been realized on single artificial synaptic devices with energy consumption of femto-Joule per event, which has limited the building of neuromorphic computing systems.[2,9]

Organometal trihalide perovskites (OTPs) including methylammonium lead iodide ($MAPbI_3$) have recently emerged as a new generation of earth abundant semiconductor materials for solar cell applications,[10–15] which have demonstrated a high certified efficiency over 20%[10] due to their superior optoelectronic properties of strong absorption,[16] unusual defect physics,[17] extremely low trap density, and long carrier diffusion length.[18] Besides, they have also been demonstrated for applications in other electronic devices, light emitting diodes,[19] laser,[20] photodetectors.[21] In this work, we demonstrated low-temperature, solution-processed two-terminal $MAPbI_3$ devices as ideal candidates of memristors and synaptic devices to mimic the biological synapses. The two-terminal OTP synaptic devices can mimic the neuromorphic learning and remembering process. Many functions of biological synapses have been visualized in the perovskite synaptic devices including four forms of spike-timing-dependent plasticity (STDP), spike-rate-dependent plasticity (SRDP) short-term plasticity (STP) and long-term potentiation (LTP)), and learning-experience behavior etc. The perovskite synapse has potential of low energy consumption of femto-Joule/(100 nm)^2 per event due to the switchable *p-i-n* structure and low activation energy for the ion migration in OTP material.[22] A novel phenomenon of photo-read SRDP was observed, which offer a novel readout method using light in addition to the electric pulse.

2. Memristic Characteristics

Figure 1a shows the structure of the device with perovskite layer sandwiched between two electrodes poly(3,4-ethylenedioxythiophene):poly(styrenesulfonate) (PEDOT:PSS) covered indium tin oxide (ITO) and gold (Au), which have comparable work functions. PEDOT:PSS is considered as an anode and Au as a cathode for the simplicity of following discussion. It is a typical metal–semiconductor–metal (MSM) structure

Dr. Z. Xiao, Prof. J. Huang
Department of Mechanical and Materials Engineering and Nebraska Center for Materials and Nanoscience
University of Nebraska-Lincoln
Lincoln, NE 68588-0526 USA
E-mail: jhuang2@unl.edu

DOI: 10.1002/aelm.201600100

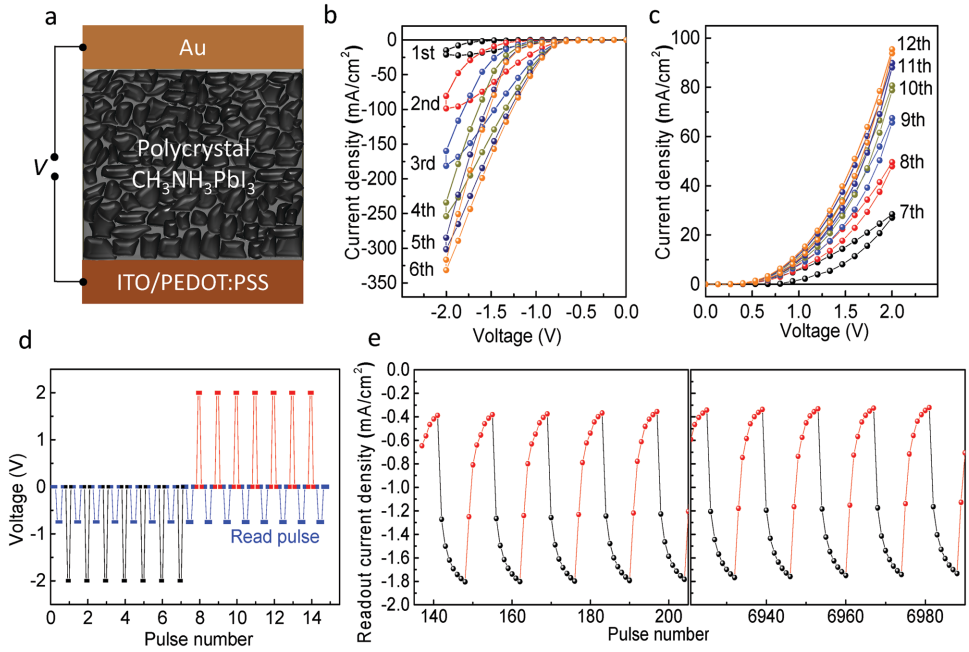

Figure 1. Memristive behavior of the OTP synaptic device. a) Schematics of the device structure. Under external applied bias, the charged ions/vacancies will migrate toward the electrode and result in doping of the perovskite near the electrode. b,c) Memristive characteristics of the device under the positive and negative biases scanning, the scanning rate is 0.1 V s^{-1}. d) Voltage trains applied on the device and e) readout current density of the device at −0.75 V read pulse. The −2.0 V and +2.0 V pulse will switch the device to *n-i-p* and *p-i-n* direction, respectively, where the readout current at −0.75 V will increase and decrease, respectively. Poling pulse duration: 0.5 s, read pulse duration: 0.5 s, time interval between the poling pulse and read pulse: 0.6 s.

device. Such a simple sandwich structure is good for building large-scale synaptic arrays.[1] It was reported that the halide containing perovskites are good ion conductors.[23–26] In our previous study of OTP photovoltaic devices, giant switchable photovoltaic effect was observed because the ion migration in OTP layer induced the formation of switchable *p-i-n* structure.[27] Positive bias pulses (or spikes, defined as electric field pointing from PEDOT:PSS to Au) cause the migration of positively charged $V_I^{\bullet}$ or $MA_i^{\bullet}$ to the Au side and/or negatively charged V'_{MA} or V'_{Pb} to the PEDOT:PSS side.[22,27] Therefore, the diode polarity of the device will be switched to *p-i-n* direction with *p*-type doping region near the PEDOT:PSS and *n*-type doping region near the Au, respectively. Negative bias pulses switch the device to *n-i-p* direction. It has been demonstrated that the switching time is correlated to the morphology of the hybrid perovskite films. An OTP film with smaller grains makes the switching easier, because the ion migration is much faster along grain boundary due to its more open structure.[27] In this study, the perovskite film with a thickness of 300 nm was annealed at 100 °C for 30 min, which was shorter than the optimized annealing time of 1–2 h for solar cells,[28] to intentionally increase the grain boundary density in the films to facilitate the ion migration for memristor and synapse applications.

The memristive characteristics of the devices in the dark are shown in Figure 1b,c. When consecutive negative bias (0 to −2.5 V) sweeps were applied on the device, the amplitude of dark current continuously increased. This indicates that the negative bias scanning gradually switches the device to *n-i-p* polarity because negative bias works as forward bias for the *n-i-p* polarity. When consecutive positive (0–2.5 V) sweeps were applied on the devices, the dark current also continuously increased, indicating that positive bias scanning gradually switches the device to *p-i-n* polarity because positive bias works as forward bias for the *p-i-n* polarity. It also should be noted that there might be a small Schottky barrier at both sides of the device before poling at the MS interfaces. After positive bias poling, the device will be poled to *p-i-n* direction. In this case, the electron injection barrier at the cathode side and/or the hole injection barrier at the anode side will be smaller. Therefore, the current density of the device would be larger at positive bias after positive poling compared with the case that there is no ion migration. As a result, the shift of the Fermi level due to the formation of the *p-i-n* structure will benefit for the memristic effect. The conductivity/resistance of the devices could also be gradually tuned by applying a train of poling spikes, which is a typical behavior of memristors. Figure 1d shows the applied poling spikes with fixed amplitude of 2 V or −2 V, and read pulses of −0.75 V. The read voltage was selected at −0.75 V because of the largest on–off ratio of the devices around −0.75 V, as shown in Figure S1 (Supporting Information). Figure 1e shows the current density readout at ≈0.75 V. The negative voltage spikes tend to switch the device to *n-i-p* direction, which results in increased readout current, while the positive spikes tend to switch the device to *p-i-n* polarity, which results in decreased readout current. The conductivity of the device has been repeatedly tuned for more than 500 cycles. The fluctuations of the conductivity at each of the seven states measured in Figure 1e are between 9.4% and 14.6%.

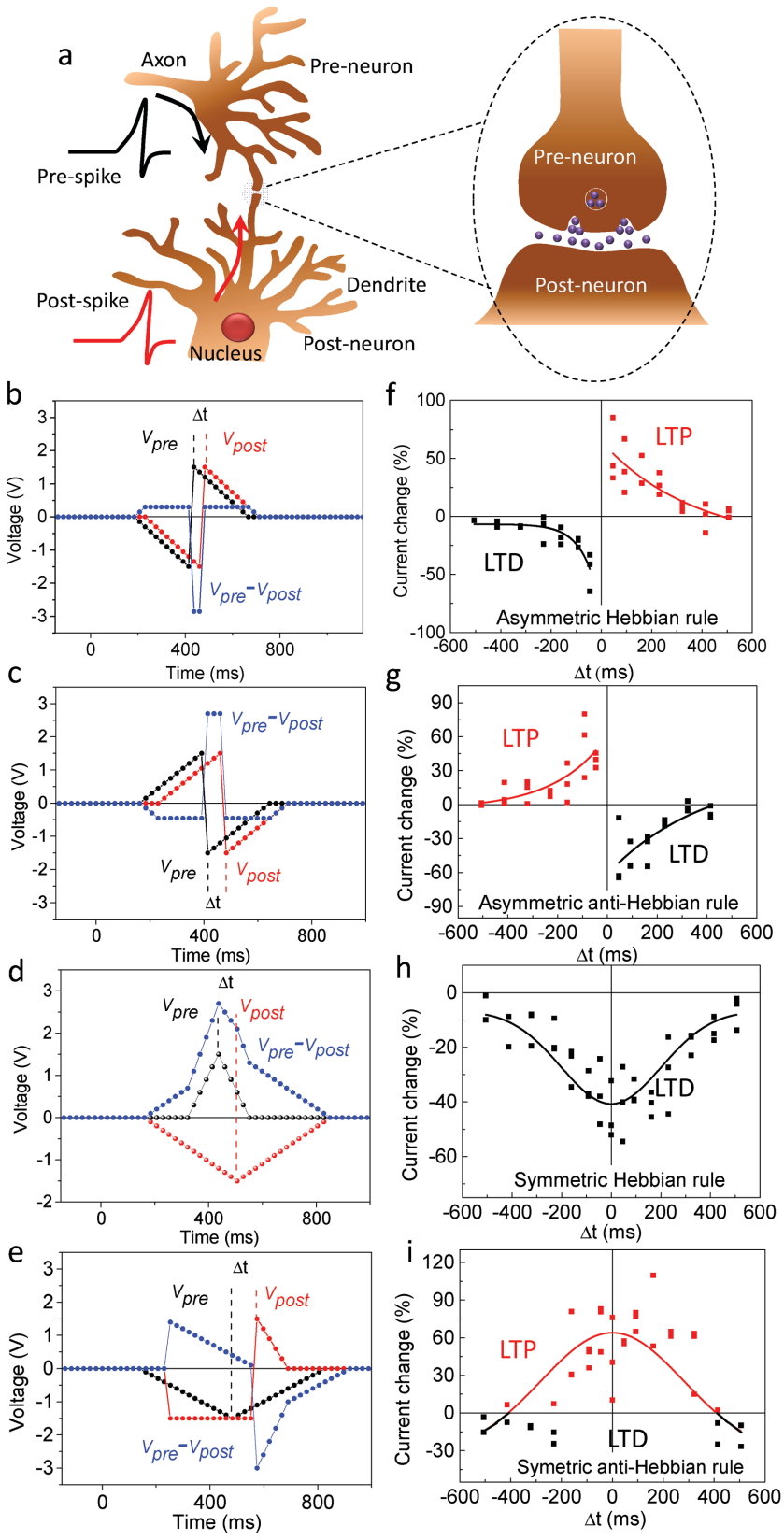

Figure 2. STDP of the OTP synaptic device measured in the dark. a) Schematics of a biological synapse. The voltage spikes for b) asymmetric Hebbian rule, c) asymmetric anti-Hebbian rule, d) symmetric Hebbian rule, and e) symmetric anti-Hebbian rule. The total voltage applied on the device at each time point is defined by the voltage difference between the pre-spike and post-spike (V_{pre}–V_{post}). The conductivity of the device was read by –0.75 V pulse before and after the spike pairs with interval of 3 s, which is "short term" measurement and during the decay process. Four forms of STDP, f) asymmetric Hebbian rule $\left(\Delta W = A\exp\left(-\frac{\Delta t}{\tau}\right) + W_0\right)$ (τ = 100–300 ms), g) asymmetric anti-Hebbian rule $\left(\Delta W = A\exp\left(-\frac{\Delta t}{\tau}\right) + W_0\right)$ (τ = 200–300 ms), h) symmetric Hebbian rule $\left(\Delta W = A\exp\left(-\frac{\Delta t^2}{2\tau^2}\right) + W_0\right)$ (τ = 200 ms) and i) symmetric anti-Hebbian rule $\left(\Delta W = A\exp\left(-\frac{\Delta t^2}{2\tau^2}\right) + W_0\right)$ (τ = 80 ms). The increase of conductivity after each pre- and post-spike pair will lead to LTP of the synaptic device, while decrease of conductivity after each pre- and post-spike pair lead to LTD.

3. Synaptic Functions

3.1. Spiking-Timing-Dependent Plasticity

Biological synapse acts as a bridge to transmit electrical or chemical signals between two nerve cells.[9] A biological synapse is composed of a pre-synaptic neuron, a post-synaptic neuron, and a synapse, as illustrated in **Figure 2**a. In artificial synaptic devices made of memristors, the bottom and top electrodes work as the pre- and post-synaptic neurons, respectively.[4,9] The conductivity/resistance of the devices represents connection strength between the neurons (synaptic weight), and the increase or decrease of conductivity/resistance represents potentiation or depression of the synaptic weight in response to the potentiating and depressing spikes. Synaptic plasticity is the basis of learning and memory in the brain,[29] referring to the change of synaptic weight (ΔW) over time in response to the activity spikes. One essential function of the synapse is spike-timing-dependent plasticity (STDP), also known as Hebbian learning rule, referring to the sign and magnitude of the synaptic weight change is closely related to the relative timing between the pre- and post-spikes. Four forms of STDP behaviors have been discovered in the biological synapse.[1,30] They have different functions regarding to the information processing and storage, which are indispensable in neural circuit design.[31,32] Taking the most famous asymmetric Hebbian learning rule as an example, when a post-synaptic spike arrives momentarily (milliseconds) after the pre-synaptic spike ($\Delta t > 0$, $\Delta t = t_{post} - t_{pre}$), the spikes will lead to long-term potentiation (LTP) of the synapse, which is represented by the increase of conductivity in the artificial

synaptic devices. Repeated post-synaptic spike before pre-synaptic spikes ($\Delta t < 0$) leads to long-term depression (LTD) represented by the decrease of conductivity in the artificial synaptic devices. The shape of pre-spike and post-spike applied on the devices is shown in Figure 2b–e. The total voltage applied on the device is defined as $V_{pre}-V_{post}$. Figure 2f–i shows the readout current change at –0.75 V versus the timing difference Δt between pre-spike and post-spike in our OTP devices. Four different forms of STDP were realized in these OTP synapses by modifying the shape of the pre-synaptic and post-synaptic spikes. The key idea of realization of different types of STDP is to translate timing difference into voltage amplitude difference. The ΔW of asymmetric Hebbian and anti-Hebbian can be fitted by the equation of $\Delta W = A\exp\left(-\frac{\Delta}{\tau}\right)+W_0$, and that of the symmetric Herbian and anti-Hebbian behavior (Figure 2d,e) can be fitted by a Gaussian function of $\Delta W = A\exp\left(-\frac{\Delta t^2}{2\tau^2}\right)+W_0$, where τ is the fitted time constant of the synaptic function, A and W_0 are constants.[32] It is noted that the τ of our OTP synaptic devices for different STDP forms are ≈80–300 ms, which is in the same range with biological synapses.[9]

3.2. Spiking-Rate-Dependent Plasticity

The SRDP, another essential function of the synapses,[33] was also demonstrated in our OTP devices. In analogy to biological synapses, the OTP device showed short-term plasticity (STP) where the device rapidly returned to its original state when the interval between the repetition spikes was long, and long-term potentiation (LTP) where the device conductivity changed when the interval between the repetition spikes was short. The devices were preset at *p-i-n* direction so that the readout current at –0.75 V was small due to the small reverse-bias saturation current of the *p-i-n* structure. **Figure 3**a,b show two trains of spikes applied on the devices, which include ten poling spikes with amplitude of 2.5 V and an interval of 20.1 s or 1.5 s, respectively, and duration of 0.8 s. In order to avoid additional poling effect by the read spikes, the read spikes were only applied on the devices before and after the train of poling spikes. The STP and LTP functions of the OTP devices can be observed by comparing the dark current at different ranges as shown in Figure 3c,d. First, the backflow current peaks after each poling spike measured at zero bias, shown in panel I, explained the origin of the STP and LTP function of the device. The amount of charges calculated by integrating the peak is around 1.4×10^{13} cm^{-2}, which is much larger than the discharge of the capacitor of around 2.6×10^{12} cm^{-2}. And the decay time of the peak (≈5 s) is much longer than the resistance–capacitance time constant of the device (microseconds range, considering the device resistance: 50 ohm•cm^2, capacitance: 170 nF cm^{-2}). Therefore, those dark current peaks should be attributed to the back diffusion of charged ions/vacancies. When the applied voltage spikes have an interval of 20.1 s, the backflow current decreased to zero before the next poling spike came in. So the drifted ions/vacancies could diffuse back, which compensated the drift effect under the applied spikes. However, when the next spike came before the back diffusion finished, the continuously applied spikes induced the net diffusion of ions/vacancies. After ten short-interval spikes, the device was switched from *p-i-n* to *n-i-p* polarity. Second, the readout current at –0.75 V, shown in panel II, directly shows the STP and LTP function of the OTP synaptic devices. After poling by the voltage spikes with the long interval of 20.1 s, the readout current density of the device kept almost unchanged at 5.5×10^{-3} mA cm^{-2}, which is the STP function. On the contrary, after poling by the

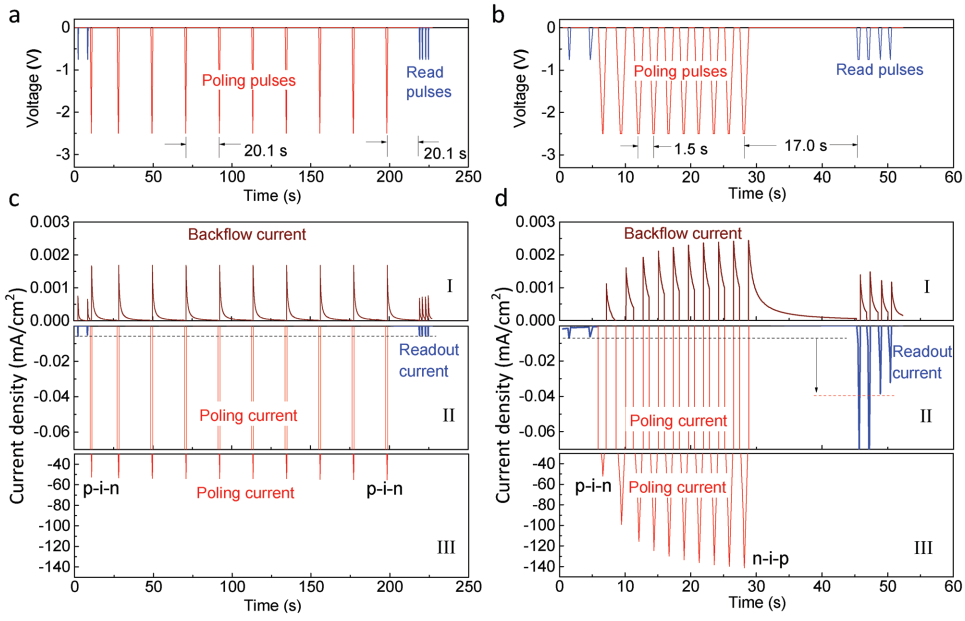

Figure 3. SRDP of the OTP synaptic device measured in the dark. Voltage trains applied on the device with a) long-time interval and b) short-time interval between the spikes. The duration of each spike is 0.8 s. The read spikes were only applied before and after the poling spikes to avoid additional poling of the device. c,d) The measured dark current through the device. The three panels show different range of the measured current. Panel I: back diffusion of the charged ions/vacancies at zero bias; Panel II: the readout dark current at –0.75 V; Panel III: Poling current at –2.5 V poling bias.

voltage spikes with the short interval of 1.5 s, the dark current increased to 4.9×10^{-2} mA cm^{-2}, which is the LTP function. It is noted that the readout current was decreasing with time. It is exactly the famous function of forgetting and remembering of human brain. Third, the poling current at –2.5 V in panel III, which includes the leakage current and ion migration current, also showed STP and LTP behaviors. For the long-interval poling spikes, the poling current kept almost unchanged, which indicates the device kept at *p-i-n* polarity. However, for the short-interval poling spikes, the poling current increased gradually from 60.0 to 141.0 mA cm^{-2}, indicating that the device was switched gradually from *p-i-n* to *n-i-p* polarity.

The photovoltaic effect in these OTP synaptic devices enabled a novel readout method of SRDP by light. The device with *p-i-n* and *n-i-p* structure can output an open-circuit voltage (V_{OC}) of 0.50 V and –0.75 V, respectively, under one sun illumination, as shown in Figure S2 (Supporting Information). A train of 20 poling pulses with long interval of 5.0 s or short internal of 0.8 s were applied on the device, and the V_{OC} of the device after each poling spike was recorded. The duration of each poling spike is 0.12 s. **Figure 4**a,b show the performance of the device preset at *p-i-n* polarity with negative poling spikes, and Figure 4c,d show the device performance preset at *n-i-p* polarity with positive poling spikes. It is clear that the poling spikes with long interval could not switch the device, which is an STP behavior, while the poling pulses with short interval switched the device, consistent with the LTP behavior. The statistics of V_{OC} of the device based on ten devices of each category are shown in Figure 4e,f. It should be noted that our OTP synaptic devices measured at V_{OC} condition worked as bi-stable memristors, both the *p-i-n* and *n-i-p* structures are stable under light illumination, which is different from the readout current shown in panel II of Figure 3d. The stable readout photovoltage is due to the light poling effect of the perovskite device.[34] The photovoltage works in the same way as the applied external bias. The photovoltage-induced additional electric field can also cause drift of the ions/vacancies; the migration of ions will increase the doping level of the perovskite materials, which results in the photovoltage increase.[34] The drift of ions will stop when it is balanced by the back diffusion of ions. The photovoltaic property of the OTP synaptic device may have potential application in visual information prosthesis. The OTP device can detect light and the generated photovoltage 0.5–0.8 V is high enough to stimulate the retinal ganglion cells. Therefore, the photodetection by the photoreceptor and signal processing by the synapse in human visual system can potentially be combined together in single OTP synaptic device. The current response speed is shorter than 0.1 ms (Figure S3, Supporting Information), which is much faster than the speed of processing in the human visual system of 150 ms.[35] Another advantage of $MAPbI_3$ materials is that its absorption covers the whole visible light up to 800 nm, which matches well with that of human eyes.

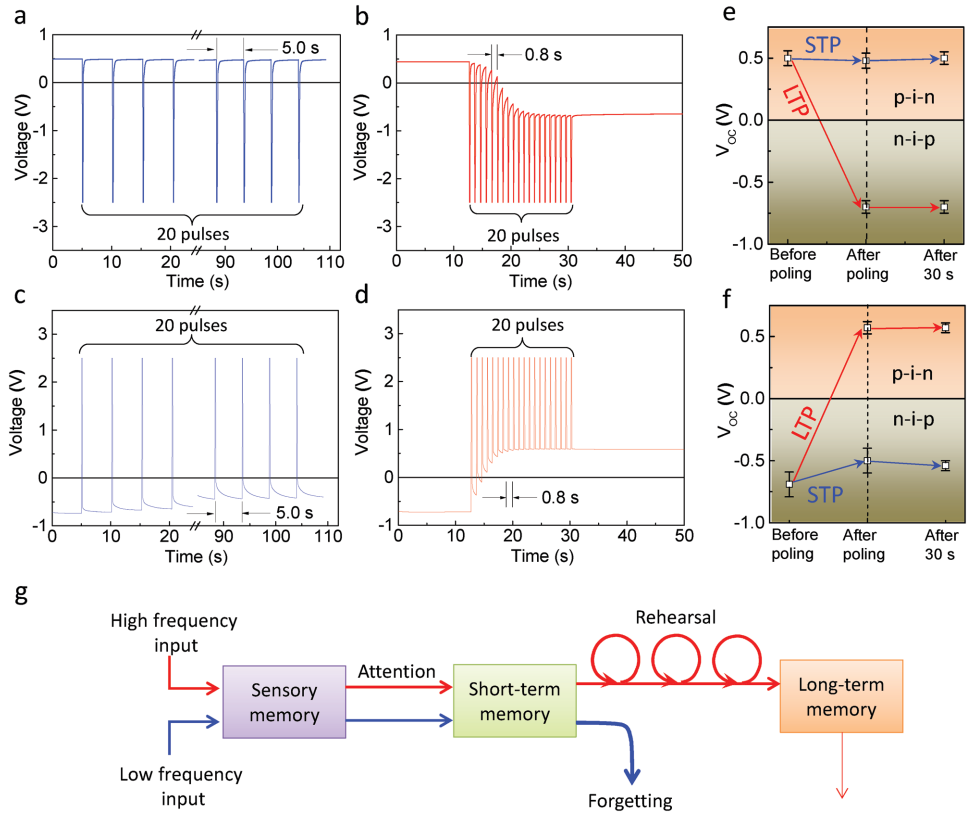

Figure 4. Photo-read SRDP of the OTP synaptic device measured under one sun illumination. a,b) The photo-read SRDP of the device with the device preset at *p-i-n* polarity. c,d) The photo-induced SRDP of the device with the device preset at *n-i-p* polarity. The duration of each poling spike is 0.12 s. After each spike, the V_{OC} of the devices were recorded. e,f) Statistics of the V_{OC} before and after the spike trains, and 30 s after the spike trains. g) Schematics of the psychological model of human memory proposed by Atkinson and Shiffrin.[36]

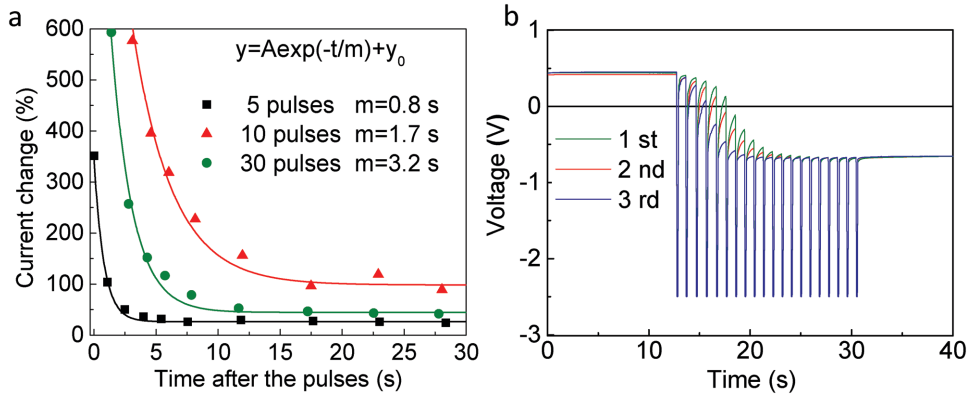

Figure 5. Forgetting and learning-experience behavior of the OTP synaptic devices. a) Forgetting behavior of the OTP synaptic devices. The poling voltage of each pulse is –2 V (duration: 0.2 s), the time interval between each pulse is 1.5 s. The device was read at –0.75 V. The curves were fitted by exponential decay. The memory retention increased with the number of rehearsals (pulses). b) The learning-experience behavior of the OTP synaptic devices. The pulse duration is 0.12 s, the time interval between pulses is 0.8 s.

3.3. Forgetting and learning behavior

Both the electric-read SRDP in the dark and photo-read SRDP under light illumination are in high similarity with the psychological model proposed by Atkinson and Shiffrin regarding to the remembering and forgetting process in human brain.[33,36] As illustrated in Figure 4g, information detected by the sense organs enter the sensory memory (SM), all the information paid attention to is transferred to short-term memory (STM), and is stored for a short time. Frequent rehearsal before complete forgetting results in long-term memory (LTM), while rehearsal with long-time interval leads to STM. Similar to the psychological model, spikes with short interval (representing frequent rehearsal) can change the diode polarity of the OTP synaptic devices (representing LTM) while the spikes with long interval cannot change the diode polarity of the devices (representing STM), as shown in Figure 3 and Figure 4a–f. The forgetting process of the device measured in the dark is shown in **Figure 5**a.

The learning-experience behavior of human was also demonstrated in OTP synaptic device. As shown in Figure 5b, three poling cycles with short-time interval of 0.8 s were applied on the device to examine how fast the device can be switched from *p-i-n* to *n-i-p* polarity. After each cycle, the device was set to *p-i-n* polarity again by applying a +2 V pulse for several seconds. This process is different form some other reports that the synaptic weight relax to a mid-state after the initial learning process and less number of pulsed was need to achieve the synaptic weight change for the re-learning process.[2] The device can be switched more easily at the third poling cycle. This indicates that, the device can do the learning process faster after the original information was forgotten.

4. Energy consumption

The OTP synaptic device based on switchable *p-i-n* structure caused by the ion-migration-induced doping is distinct from other reported synaptic devices based on phase change,[37] ferroelectric tunnel junction,[38] ion-motion-induced resistive change,[39] and atomic conduction bridge.[33] It is noted that the doping effect needs only parts per million (ppm) range atoms. It is more efficient than the synaptic devices based on conducting bridge effect and ion-motion-induced resistivity change, which require the migrated ions form conducting filaments.[9,39] The switchable *p-i-n* structure results in low energy consumption of the perovskite device due to the small amount of atoms needed for the doping and low activation energy of 0.36 eV for the ion migration in OTP material.[22] The main energy consumption is from the poling process due to the large poling current. The device resistance can be modulated at higher voltage with much shorter poling time, which can potentially reduce energy consumption. As shown in **Figure 6**, the readout current of the device at –0.75 V increased by 100% after poling by –11 V bias for 100 µs. The poling current was 500 mA cm^{-2}, corresponding to a poling energy consumption of 0.3 J per event, which indicates it has potential of low energy consumption of 55 fJ for a device area of $(100\ nm)^2$ supposing a linear relationship of the poling current with the device area. The vertical structure device with small device area cannot be fabricated currently because both the resist and developer solution can damage the perovskite film. Nevertheless, the lateral structure device might also be a good choice for the synaptic device. In our previous work, the lateral structure devices were fabricated by depositing lateral gold electrode bars with different channel length from 100 to 8 µm using photolithography, followed by spin coating of perovskite layers on top.[22,27] The lateral structure device can also be gradually switched by a small electric field of 1.5 V $µm^{-1}$, which is similar with the vertical structure device.[22] Considering that the human brain has more than 10^{14} synapse, the lateral structure device can make the building of the synaptic network much easier than the vertical structure devices. Although the processing speed of 100 µs of OTP synaptic device is slower than ferroelectric memristor (accumulation of 300 ns of 2.7 V pulse for resistivity change of 100%)[38] and phase change memristor[37] (accumulation of 5 µs of 2–4 V pulse for resistivity change of 100%), it is already three orders faster than the processing speed of human brain of 100 ms range. The advantage of brain-inspired computation is its parallel computing. Both the processing speed and

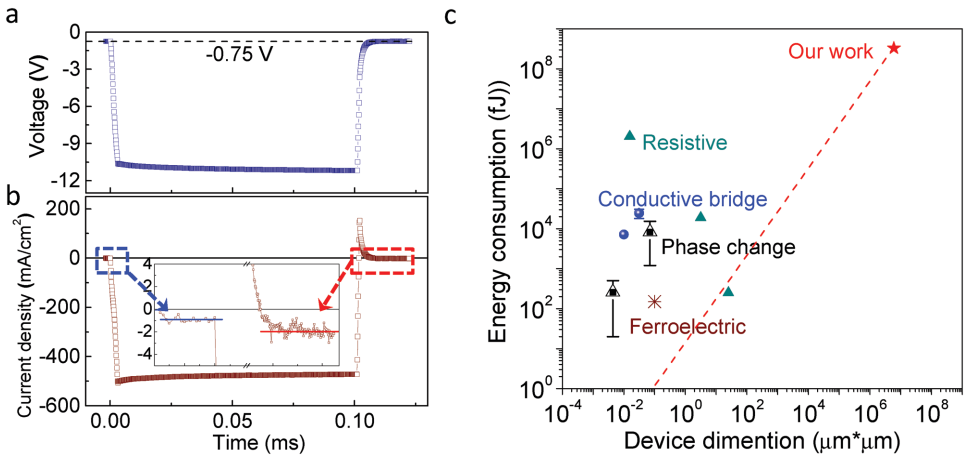

Figure 6. The energy consumption of OTP synaptic device. Voltage pulse applied on the a) device and b) measured current. c) The energy consumption of our device compared with reported values from ref. [9]. The red dash line shows the potential energy consumption of the device with small area supposing linear relation of the poling current with the device area. The readout current increased from 1.0 to 2.0 mA cm^{-2} after the poling pulse which corresponding to 100% change of the conductivity. The positive current peak just after the poling spike is due to the discharging of the device.

the energy consumption can be potentially decreased by composition and/or morphology engineering of the OTP layer to decrease the charge carrier conductivity as well as increase the ion conductivity.

It might be possible that the ion motion in the perovskite layer toward the electrode may cause conductivity change of the PEDOT:PSS layer.[40] But this should play a neglected role in our perovskite memristor devices. One direct evidence is that, for PEDOT:PSS memristor, the positive and negative biases will increase and decrease the device conductivity, respectively, due to the migration of metal atoms into and back from the PEDOT:PSS layer.[40] But for our perovskite memristors, both positive and negative biases increase the device conductivity. This is because the negative bias (defined in the main text) switches the device to *n-i-p* polarity, and then negative bias works as FORWARD bias. Similarly positive bias switches the device to *p-i-n* polarity, and then positive bias works as FORWARD bias. Therefore, the conductivity/resistivity change of the perovskite memristor mainly results from the switchable *p-i-n* structure. In addition, the device without PEDOT:PSS layer, with a structure of ITO/$MAPbI_3$/Au also shows memristic behavior, as shown in the Figure S4 (Supporting Information). This also proves that PEDOT:PSS does not contribute to the memory characteristics of the perovskite memristor devices.

5. Conclusion

In summary, we demonstrated that the ion-conducting OTP materials are ideal candidates for memristor and synaptic devices, which can mimic the biological synapse. Compared with other reported materials including oxides, chalcogenides, and Si-based materials, the advantages of OTP materials rely on its low-cost, solution processable, low activation energy for ion migration and formation of switchable *p-i-n* structure, etc. In addition to $MAPbI_3$, other OTP materials including $MAPbBr_3$, $FAPbI_3$, $MAPbI_3Cl_{3-x}$ etc. and inorganic lead halide perovskites like $CsPbI_3$ were also demonstrated to be ion conducting materials,[23,27] which can also be used for memristor and synaptic devices. Those perovskite materials have lower or comparable conductivity with $MAPbI_3$ so that they can also potentially operate with low energy consumption. Further improvement should be to decrease the dimension of the device using photolithography technique, and further decrease the energy consumption to sub-femto-Joule per event by device and materials engineering.

Experimental Section

PEDOT:PSS (Baytron-P 4083) was spin-coated on clean ITO substrates at a speed of 3000 rounds per minute (rpm). The films were then annealed at 105 °C for 30 min. Lead iodide (PbI_2) and methylammonium iodide (MAI) were first dissolved in dimethylformamide (DMF) and 2-propanol, respectively. The $MAPbI_3$ films were formed by spin coating PbI_2 (450 mg mL^{-1} in DMF) and (50 mg mL^{-1} in 2-propanol) sequentially at 6000 rpm for 35 s respectively at room temperature, followed by thermal annealing at 100 °C for 30 min. The devices were finished by the thermal evaporation of 50 nm Au as electrode. The device area is 0.06 cm^2.

A Keithley 4200 semiconductor analyzer was used to apply scanning bias and test the output current simultaneously. The pulse mode function of Keithley 4200 was used for the pulse mode measurement in Figure 6, other measurements used the function of current or voltage list scanning, where the lists can be programmed manually. All the electrical tests for vertical devices were conducted in glove box. For the photo-read SRDP, the devices were measured under AM 1.5 G illumination (100 mW cm^{-2}) using a Xenon-lamp-based solar simulator (Oriel 67005, 150 W Solar Simulator).

Supporting Information

Supporting Information is available from the Wiley Online Library or from the author.

Acknowledgements

The authors thank the National Science Foundation for its financial support under Awards ECCS-1252623 and DMR-1420645.

Received: March 8, 2016
Revised: April 5, 2016
Published online:

[1] Y. Li, Y. Zhong, J. Zhang, L. Xu, Q. Wang, H. Sun, H. Tong, X. Cheng, X. Miao, *Sci. Rep.* **2014**, *4*, 4906.
[2] Z. Q. Wang, H. Y. Xu, X. H. Li, H. Yu, Y. C. Liu, X. J. Zhu, *Adv. Funct. Mater.* **2012**, *22*, 2759.
[3] D. B. Strukov, G. S. Snider, D. R. Stewart, R. S. Williams, *Nature* **2008**, *453*, 80.
[4] S. H. Jo, T. Chang, I. Ebong, B. B. Bhadviya, P. Mazumder, W. Lu, *Nano Lett.* **2010**, *10*, 1297.
[5] F. Alibart, S. Pleutin, D. Guérin, C. Novembre, S. Lenfant, K. Lmimouni, C. Gamrat, D. Vuillaume, *Adv. Funct. Mater.* **2010**, *20*, 330.
[6] L. Q. Zhu, C. J. Wan, L. Q. Guo, Y. Shi, Q. Wan, *Nat. Commun.* **2014**, *5*, 3158.
[7] K. Kim, C. L. Chen, Q. Truong, A. M. Shen, Y. Chen, *Adv. Mater.* **2013**, *25*, 1693.
[8] Y. H. Liu, L. Q. Zhu, P. Feng, Y. Shi, Q. Wan, *Adv. Mater.* **2015**, *27*, 5599.
[9] D. Kuzum, S. Yu, H. P. Wong, *Nanotechnology* **2013**, *24*, 382001.
[10] M. A. Green, K. Emery, Y. Hishikawa, W. Warta, E. D. Dunlop, *Prog. Photovoltaics* **2015**, *23*, 1.
[11] N. J. Jeon, J. H. Noh, W. S. Yang, Y. C. Kim, S. Ryu, J. Seo, S. I. Seok, *Nature* **2015**, *517*, 476.
[12] M. Liu, M. B. Johnston, H. J. Snaith, *Nature* **2013**, *501*, 395.
[13] J. Burschka, N. Pellet, S.-J. Moon, R. Humphry-Baker, P. Gao, M. K. Nazeeruddin, M. Grätzel, *Nature* **2013**, *499*, 316.
[14] M. M. Lee, J. Teuscher, T. Miyasaka, T. N. Murakami, H. J. Snaith, *Science* **2012**, *338*, 643.
[15] J.-H. Im, C.-R. Lee, J.-W. Lee, S.-W. Park, N.-G. Park, *Nanoscale* **2011**, *3*, 4088.
[16] A. Kojima, K. Teshima, Y. Shirai, T. Miyasaka, *J. Am. Chem. Soc.* **2009**, *131*, 6050.
[17] W.-J. Yin, T. Shi, Y. Yan, *Appl. Phys. Lett.* **2014**, *104*, 063903.
[18] Q. Dong, Y. Fang, Y. Shao, P. Mulligan, J. Qiu, L. Cao, J. Huang, *Science* **2015**, *347*, 967.
[19] Z.-K. Tan, R. S. Moghaddam, M. L. Lai, P. Docampo, R. Higler, F. Deschler, M. Price, A. Sadhanala, L. M. Pazos, D. Credgington, *Nat. Nanotechnol.* **2014**, *9*, 687.
[20] G. Xing, N. Mathews, S. S. Lim, N. Yantara, X. Liu, D. Sabba, M. Grätzel, S. Mhaisalkar, T. C. Sum, *Nat. Mater.* **2014**, *13*, 476.
[21] L. Dou, Y. M. Yang, J. You, Z. Hong, W.-H. Chang, G. Li, Y. Yang, *Nat. Commun.* **2014**, *5*, 1.
[22] Y. Yuan, J. Chae, Y. Shao, Q. Wang, Z. Xiao, A. Centrone, J. Huang, *Adv. Energy Mater.* **2015**, *5*, 1500615.
[23] K. A. J. Mizusaki, K. Fueki, *Solid State Ion* **1983**, *11*, 203.
[24] S. V. Reenen, M. Kemerink, H. J. Snaith, *J. Phys. Chem. Lett.* **2015**, *6*, 3808.
[25] T. Y. Yang, G. Gregori, N. Pellet, M. Grätzel, J. Maier, *Angew. Chem.* **2015**, *54*, 7905.
[26] C. Eames, J. M. Frost, P. R. Barnes, B. C. O'regan, A. Walsh, M. S. Islam, *Nat. Commun.* **2015**, *6*, 7497.
[27] Z. Xiao, Y. Yuan, Y. Shao, Q. Wang, Q. Dong, C. Bi, P. Sharma, A. Gruverman, J. Huang, *Nat. Mater.* **2015**, *14*, 193.
[28] Z. Xiao, C. Bi, Y. Shao, Q. Dong, Q. Wang, Y. Yuan, C. Wang, Y. Gao, J. Huang, *Energy Environ. Sci.* **2014**, *7*, 2619.
[29] H. Markram, W. Gerstner, P. J. Sjöström, *Front. Comput. Neurosci.* **2011**, *3*, 1.
[30] L. F. Abbott, S. B. Nelson, *Nat. Neurosci.* **2000**, *3*, 1178.
[31] H. Z. Shouval, S. S.-H. Wang, G. M. Wittenberg, *Front. Comput. Neurosci.* **2010**, *4*, 19.
[32] Y. Li, Y. Zhong, L. Xu, J. Zhang, X. Xu, H. Sun, X. Miao, *Sci. Rep.* **2013**, *3*, 1619.
[33] T. Ohno, T. Hasegawa, T. Tsuruoka, K. Terabe, J. K. Gimzewski, M. Aono, *Nat. Mater.* **2011**, *10*, 591.
[34] Y. Deng, Z. Xiao, J. Huang, *Adv. Energy Mater.* **2015**, *5*, 1500721.
[35] S. Thorpe, D. Fize, C. Marlot, *Nature* **1996**, *381*, 520.
[36] R. C. Atkinson, R. M. Shiffrin, *Psychol. Learning Motiv.* **1968**, *2*, 89.
[37] D. Kuzum, R. G. Jeyasingh, B. Lee, H.-S. P. Wong, *Nano Lett.* **2011**, *12*, 2179.
[38] A. Chanthbouala, V. Garcia, R. O. Cherifi, K. Bouzehouane, S. Fusil, X. Moya, S. Xavier, H. Yamada, C. Deranlot, N. D. Mathur, *Nat. Mater.* **2012**, *11*, 860.
[39] R. Waser, M. Aono, *Nat. Mater.* **2007**, *6*, 833.
[40] S. Li, F. Zeng, C. Chen, H. Liu, G. Tang, S. Gao, C. Song, Y. Lin, F. Pan, D. Guo, *J. Mater. Chem. C* **2013**, *1*, 5292.